Available online at www.sciencedirect.com
SCIENCE DIRECT®
ELSEVIER
International Journal of Solids and Structures 43 (2006) 1437–1458
INTERNATIONAL JOURNAL OF SOLIDS and STRUCTURES
www.elsevier.com/locate/ijsolstr

Nonlinear behaviour of piezoceramics under weak electric fields. Part-II: Numerical results and validation with experiments

M.K. Samal [a], P. Seshu [b,*], S.K. Parashar [c], U. von Wagner [d], P. Hagedorn [c], B.K. Dutta [a], H.S. Kushwaha [a]

[a] *Reactor Safety Division, Bhabha Atomic Research Centre, Trombay, Mumbai 400085, India*
[b] *Department of Mechanical Engineering, Indian Institute of Technology, Powai, Mumbai 400076, India*
[c] *Department of Applied Mechanics, Technische Universität Darmstadt, 64289 Darmstadt, Germany*
[d] *Department of Applied Mechanics, Technische Universität Berlin, 10587 Berlin, Germany*

Received 17 November 2004; received in revised form 15 June 2005
Available online 24 August 2005

Abstract

When excited near resonance in the presence of weak electric fields, piezoceramic materials exhibit typical nonlinearities similar to a Duffing oscillator such as jump phenomena and presence of superharmonics in the response spectra. In an accompanying paper, a generalized nonlinear 3D finite element formulation has been developed incorporating quadratic and cubic terms in the electric enthalpy density function and the virtual work done by damping forces. In this paper, the formulation has been validated by conducting experiments on test pieces of various geometries and of three different materials (in all, four case studies). Both proportional damping and nonlinear damping formulations have been used to predict the frequency response of these systems. Newmark-β method has been used to obtain the dynamic response of the systems using FE analysis. It is demonstrated that the nonlinear finite element model is able to predict the responses of the various test cases studied and the results match very well with those of experimental observations.
© 2005 Elsevier Ltd. All rights reserved.

Keywords: Piezoceramic; Nonlinear modeling; Jump phenomena; Weak electric fields; Structural mode

* Corresponding author. Tel.: +91 2225767534; fax: +91 2225726875.
E-mail address: seshu@iitb.ac.in (P. Seshu).

0020-7683/$ - see front matter © 2005 Elsevier Ltd. All rights reserved.
doi:10.1016/j.ijsolstr.2005.06.067

1. Introduction

Piezoceramic materials are gaining worldwide attention of many researchers in recent years for different actuator and sensor applications because of their high electro-mechanical coupling coefficient. A special class of these actuators is known as ultrasonic transducers. These are usually driven at resonance frequency with very low electric fields of the order of few volts per millimeter. Under these conditions, various kinds of nonlinearities are observed such as jump phenomena, dependence of resonance frequency on vibration amplitude, presence of superharmonics in the response spectra and nonlinear relationship between applied electric voltage and mechanical displacement, etc. (Beige and Schmidt, 1982, von Wagner and Hagedorn, 2002, von Wagner, 2003, 2004). The problem associated with piezo-actuators showing the jump phenomena can be excessive heat generation, mechanical break down and instability of vibration when operating in the resonant mode, etc. The nonlinear behaviours of piezo-actuators can also affect the applications such as the active shape and vibration control of structures (Sun et al., 2004; Zhou and Tzou, 2000).

Modeling of these nonlinearities is of great importance to designers for optimization of performance of various devices operating in the said regime. In a companion paper (Samal et al., 2005), a 3D finite element (FE) formulation has been developed to model nonlinearities of piezoceramics under weak electric fields. The nonlinear FE equations obtained from variational formulation using the nonlinear electric enthalpy function as well as the virtual work done by nonlinear damping forces are obtained as

$$\begin{bmatrix} M & 0 \\ 0 & 0 \end{bmatrix}^{(t+1)} \begin{Bmatrix} \ddot{u}_i \\ \ddot{\phi}_i \end{Bmatrix}^{(t+1)} + \begin{bmatrix} K_{uu} & K_{u\phi} \\ K_{\phi u} & K_{\phi\phi} \end{bmatrix}^{(t+1)}_{\text{linear}} \begin{Bmatrix} u_i \\ \phi_i \end{Bmatrix}^{(t+1)} + \begin{Bmatrix} f_{m\_i} \\ f_{e\_i} \end{Bmatrix}^{(t+1)}_{\text{nonl}} = \begin{Bmatrix} f_i \\ g_i \end{Bmatrix}^{(t+1)}, \tag{1}$$

where $\{f_{m\_i}\}^{(t+1)}\}_{\text{nonl}}$ and $\{f_{e\_i}\}^{(t+1)}_{\text{nonl}}$ are the nonlinear mechanical and electrical force vectors. These force vectors at the current time step $(t+1)$ are then split into nonlinear stiffness as well as damping matrices after following a classical linearization technique and the final form of FE equations to be solved with Newmark-β method with iteration are as follows.

$$\begin{bmatrix} M & 0 \\ 0 & 0 \end{bmatrix}^{(t+1)} \begin{Bmatrix} \ddot{u}_i \\ \ddot{\phi}_i \end{Bmatrix}^{(t+1)} + \begin{bmatrix} C_{\text{mdamp}} & C_{\text{pdamp}} \\ e_{\text{pdamp}} & e_{\text{ddamp}} \end{bmatrix}^{(t)} \begin{Bmatrix} \dot{u}_i \\ \dot{\phi}_i \end{Bmatrix}^{(t+1)} + \begin{bmatrix} K_{uu}+K_{uud} & K_{u\phi}+K_{u\phi d} \\ K_{\phi u}+K_{\phi ud} & K_{\phi\phi}+K_{\phi\phi d} \end{bmatrix}^{(t)} \begin{Bmatrix} u_i \\ \phi_i \end{Bmatrix}^{(t+1)} = \begin{Bmatrix} f_i \\ g_i \end{Bmatrix}^{(t+1)}. \tag{2}$$

In this work, the above FE formulation has been validated by carrying out experiments on three different geometries (stator of a shell type piezomotor, rectangular plate, cylindrical rod) and piezoceramic materials (PIC 141, PIC 181 and PIC 255). Experiments have been conducted at varying field strengths to check the capability of the formulation to predict the nonlinear response. The materials PIC 141 and PIC 181 have relatively low damping coefficient as compared to PIC 255. Two different damping formulations, i.e., proportional damping and nonlinear damping have been studied for all the materials. The FE simulation results for different specimen geometries have been shown to match very well with those of experiments.

2. Solution of finite element equations using Newmark-β method with iteration

The FE Eq. (2) contains the nonlinear damping and stiffness matrices which are functions of field variables u_i, ϕ_i at the start of the current time step (i.e., t). This was done essentially to assemble the nonlinear elemental FE equations and to have a starting solution for this time step. Hence, the stiffness and damping matrices evaluated with the field variables at time (t) are initial guess matrices for obtaining an initial

solution for the field variables. Once the field variables are evaluated for this time step, the stiffness and damping matrices are updated and then the next solution for same time step is sought for Eq. (2). In this

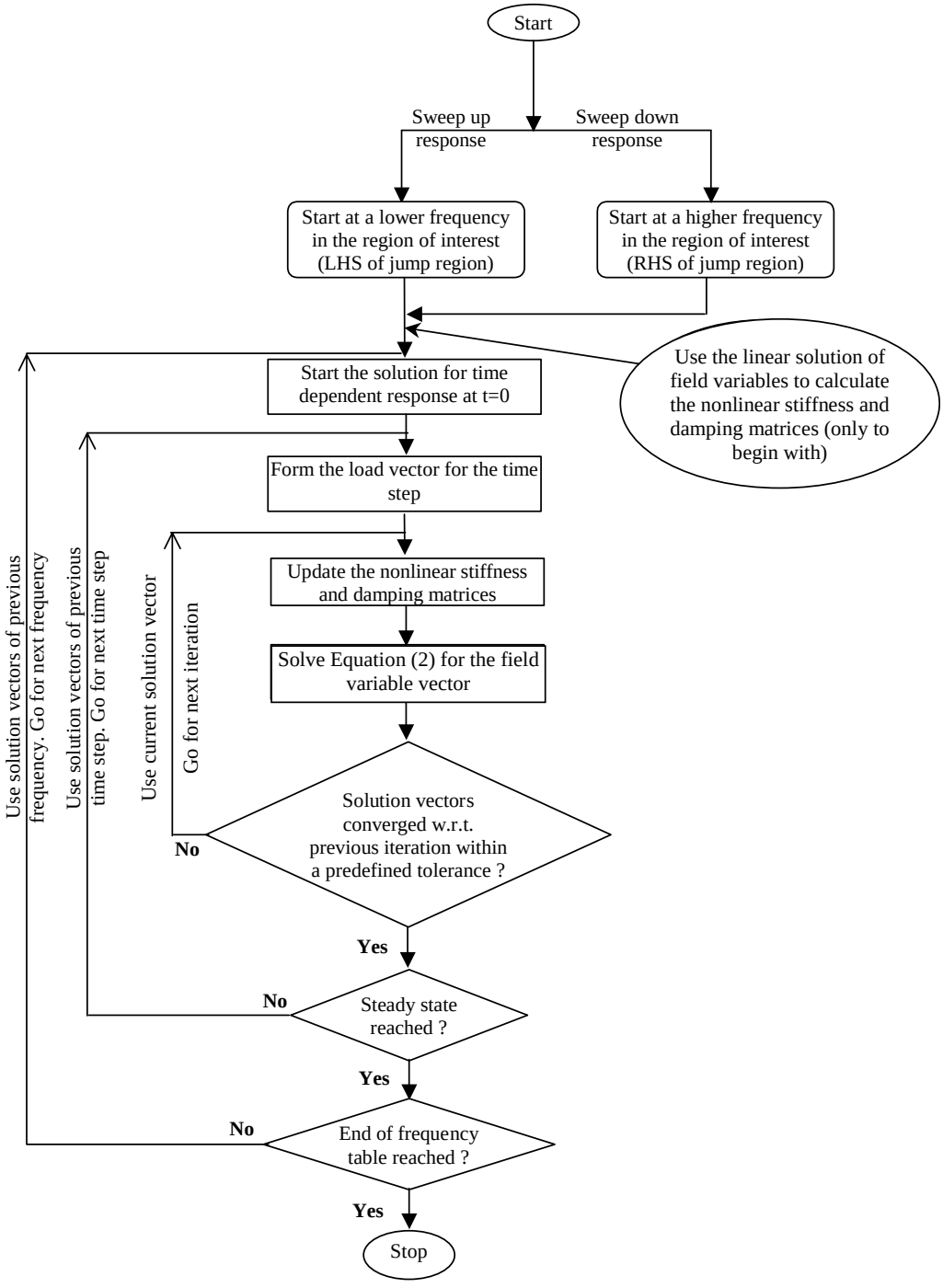

Fig. 1. Flow chart of the solution process of the set of nonlinear FE equations.

way the iterative procedure is continued till convergence in the solution of the field variable vectors is obtained within a predefined tolerance. After convergence of the solution in a particular time step, one proceeds to the next time step where the load vector is newly formed depending upon the loading condition. The converged solution for the previous time step serves as an initial approximation for the next time step. The solution procedure is repeated with time till steady state is achieved. It may be noted that all the above procedure is followed for a particular frequency of excitation.

When studying the nonlinearities under weak electric fields when excited near a structural mode, one observes jump phenomena which gets reflected in the difference of the responses in the sweep-up and sweep-down steady state solutions in the steady state amplitude versus frequency curves. In the jump region, there exist two solutions for the field variables. However, when solving using Newmark-β method, one can converge to only one solution depending upon the initial guess solution used. This characteristic helps in getting two different responses in FE analysis of sweep-up and sweep-down frequency response analysis of the piezoelectric continuum. The details of the solution procedure are shown in a flow chart in Fig. 1. It can be seen from Fig. 1 that one has to start from a lower value frequency in the region of interest where one wants to find the nonlinear frequency response. To begin with, one can use the linear solution of the field variable as an initial guess solution and proceed to iteration process as already explained. However, for the next frequency of excitation, one should use the converged steady state solutions of field variables from the immediate lower frequency of excitation as an initial guess for solution of Eq. (2) and then proceed for the iteration and then solution for steady state by following the time marching procedure. In this way one goes on increasing the frequency of excitation and will be able to trace the sweep-up nonlinear frequency response curve. For the sweep-down nonlinear frequency response solution, the procedure is just the reverse, i.e., one starts at a higher value of excitation frequency in the frequency region of interest and proceed to the lower frequencies using converged steady state solutions of the higher frequencies of excitation as initial guess solutions.

3. Analysis of different piezoelectric systems (2D and 3D) of different materials

3.1. Various systems studied

Experiments have been conducted on different systems, viz., stator of a shell type piezomotor (material PIC 141), free-free rectangular piezo-plates (two specimens made of different materials i.e., PIC 181 and PIC 255[1]) and cylindrical piezo-rods (material PIC 181). The four specimens are shown in Fig. 2. The details of specimen geometries, boundary conditions, etc. have been described in Section 4.

Shell type piezomotors are widely used in many applications such as in precision-positioning systems in robotics/mechatronics. The stator shell is excited in a suitable longitudinal mode to create a traveling wave in the circumference. The rotor, in contact with the stator through a friction material layer, rotates at a speed that depends upon the number of waves formed in the circumference of the shell and also on the magnitude of the circumferential displacement of each point contacting the rotor. This mechanism results in an inherent large reduction in the speed of the rotor thus obviating the need for speed reducers.

The shell specimen used in the experiment has nine sectors where the electrodes are situated (Fig. 2(a)). It is polarized in the radial direction. Three nearby sectors of the shell are excited with phase differences of 120° with external electrical excitation. The shell has been modeled using the present three-dimensional nonlinear finite element formulation with 8-node isoparametric brick elements. The 3D 8-noded brick

[1] All these materials, i.e., PIC 141, 181 and 255 are manufactured by PI Ceramic, Lederhose, Germany. Available from: <http://www.piceramic.de>.

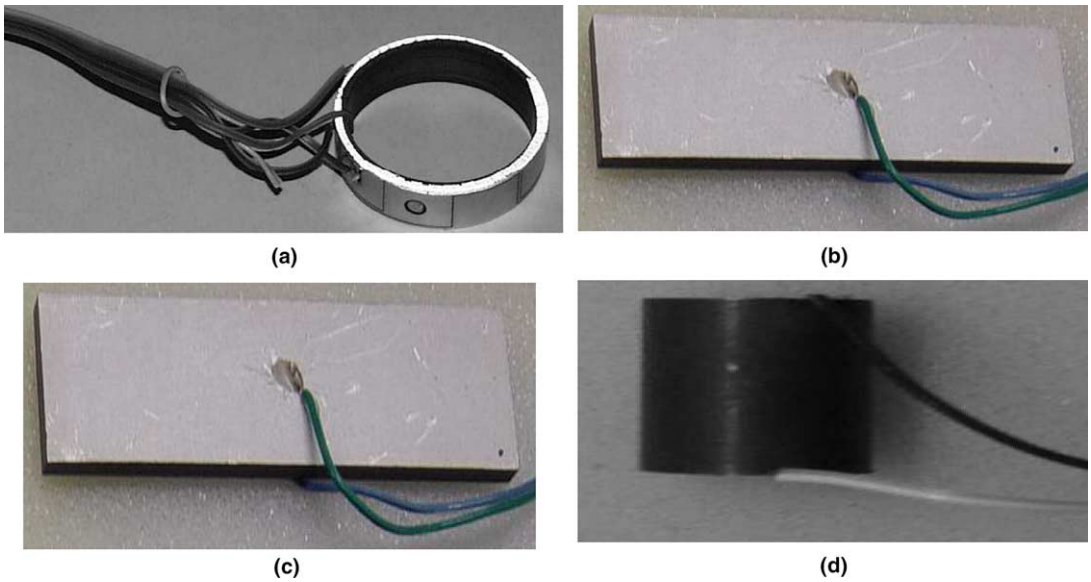

Fig. 2. Specimens used in case studies. (a) Stator of a shell type piezomotor (PIC 181), (b) free-free rectangular plate of PIC 181, (c) free-free rectangular plate of PIC 255, (d) cylindrical piezo-rod of PIC 181.

elements have 4 degrees of freedom per node i.e., mechanical displacements u, v, w in global x, y and z directions and electrical potential ϕ.

Experiments are also conducted on piezoceramic plates and cylindrical rods to study the nonlinear behaviour in their first mode of vibration (longitudinal mode for the cylindrical rod using the d_{33} piezoelectric effect and in-plane mode for the plate using d_{31} effect) for two different types of materials, i.e., PIC 181 and PIC 255. The same has been modeled using the present nonlinear finite element formulation using isoparametric, 4-node 2D plane stress/plane strain/axi-symmetric elements. The 2D 4-noded quadrilateral elements have 3 degrees of freedom per node i.e., mechanical displacements u and v in global x and y directions and electrical potential ϕ.

3.2. Experimental setup and instrumentation

All the specimens are excited close to their fundamental resonance frequencies in two ways, i.e., sweep-up (SU) and sweep-down (SD) to observe the jump phenomena. The line diagram of the experimental setup is shown in Fig. 3. The excitation and measurements have been done with the help of a gain-phase analyzer (Hewlett-Packard HP 4194A). It sends the excitation signal to the piezoceramic through a power amplifier (Bruel and Kjaer 2713). The dynamic response (velocity) signal is captured with the help of a laser vibrometer (Polytec) which is focused to one point of the structure. The vibrometer measures the velocity amplitude, which is converted to the displacement amplitude by dividing it with the applied circular frequency of excitation ω.

3.3. Convergence of finite element solution

A convergence study for the size of FE mesh to be used in the analysis was conducted for all the geometries. The mesh size was refined till the solutions of both resonance frequency as well as steady state vibration amplitude converged within a pre-defined tolerance. As an example, the results of such a study on the

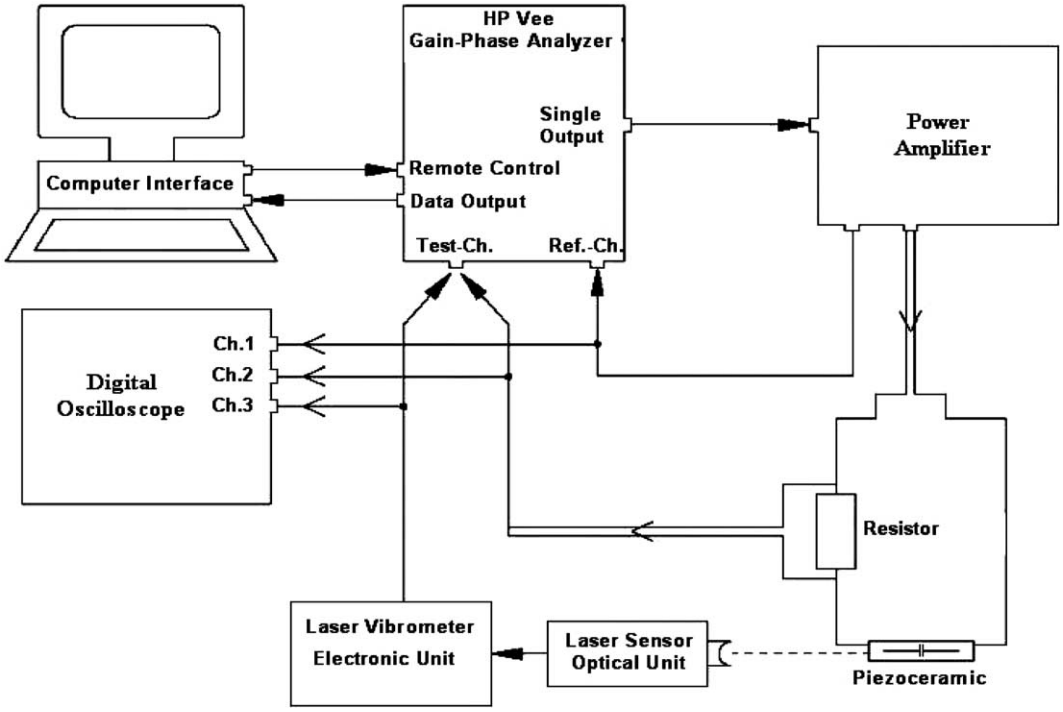

Fig. 3. Experimental setup for measuring the nonlinear dynamic response of different piezoceramic specimens.

PIC 255 plate (Fig. 2(c)) for frequency as well as steady state nonlinear response calculation (when excited at the first longitudinal mode) are shown in Tables 1 and 2, respectively. Based on the mesh convergence study, 5×5 mesh (i.e., 5 equal divisions along length and width directions for the PIC 255 plate) is chosen for the further solution process.

Similarly, the effect of time step ΔT chosen in the Newmark-β method of solution on the steady state amplitude was studied. The variation of steady state amplitude with number of time steps in a period T_1

Table 1
Mesh convergence study for the frequency calculation of PIC 255 plate

Natural frequency (kHz)	No. of elements in length and width direction						
	1×1	2×1	3×1	4×1	5×1	5×3	5×5
Mode 1	21.452	20.006	19.711	19.608	19.559	19.554	19.554
Mode 2	76.848	64.925	61.683	59.539	58.430	57.221	57.064

Table 2
Mesh convergence study for the steady state displacement amplitude (micron) of PIC 255 plate at 19.554 kHz

No. of elements in length and width direction					
3×1	5×1	5×2	5×3	5×4	5×5
1.1334	0.9442	0.9442	0.9441	0.9440	0.9437

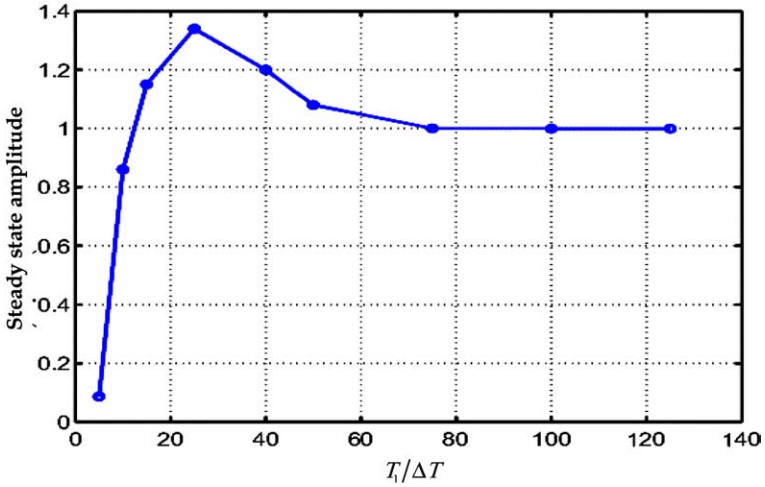

Fig. 4. Variation of steady state vibration amplitude with time increment for PIC 255 plate.

is shown in Fig. 4. It can be seen that when the time step was chosen as 75th part of a period of oscillation corresponding to the mode of vibration, convergence in the results was achieved and this value was used for the further analysis of all the specimens.

4. Results and discussion

4.1. Case study 1: Stator of a shell type piezomotor (PIC 141)

Berg et al. (2004) studied the behaviour of the stator (Fig. 2(a)) of a shell type piezomotor using Flügge's (1962, 1973) shell theory. The stator is a hollow thin cylindrical shell with 34 mm internal diameter, 2 mm thickness and 10 mm length. The shell has 12 sectors along the circumference direction which are electrically separated. This is in order to apply electric field (across the thickness) in the nearby sectors at phase differences of 0°, 120° and 240°, respectively so that a traveling wave can be generated in the annular end of the shell. The shell is vibrating in the free-free mode and hence there is no mechanical boundary condition applied. The electrical boundary conditions are prescription of the applied electrical potential ϕ at the outside and inside surface of the sectors which were excited electrically (Figs. 2(a) and 5). In this work, the shell has been excited with the help of a gain phase analyzer. A phase shifter is used to supply the input excitation to the three nearby sectors at phase angle of 0°, 120° and 240°, respectively (Fig. 5). The response is measured with the help of a laser vibrometer (focused at one point on to one end of the shell along the length direction) and the output signal is fed back to the gain phase analyzer and is compared with the reference input signal. The experiments are conducted by changing the frequencies in 400 steps between 85 and 90 kHz.

The 3D finite element mesh and mode shape for the first mode of vibration (contraction and expansion in the length direction) are shown in Figs. 5 and 6, respectively. In the analysis, 240 3D 8-noded brick elements have been used (2 in thickness direction, 10 in length direction and 12 in circumference direction). The calculated frequencies for first and second modes of vibration are shown in Table 3 and compared with the experimental frequencies and also with the frequencies calculated theoretically by Berg et al. (2004). The linear and nonlinear material properties of PIC 141 required for the finite element analysis have been taken from Samal (2003) and are given in Appendix A1.

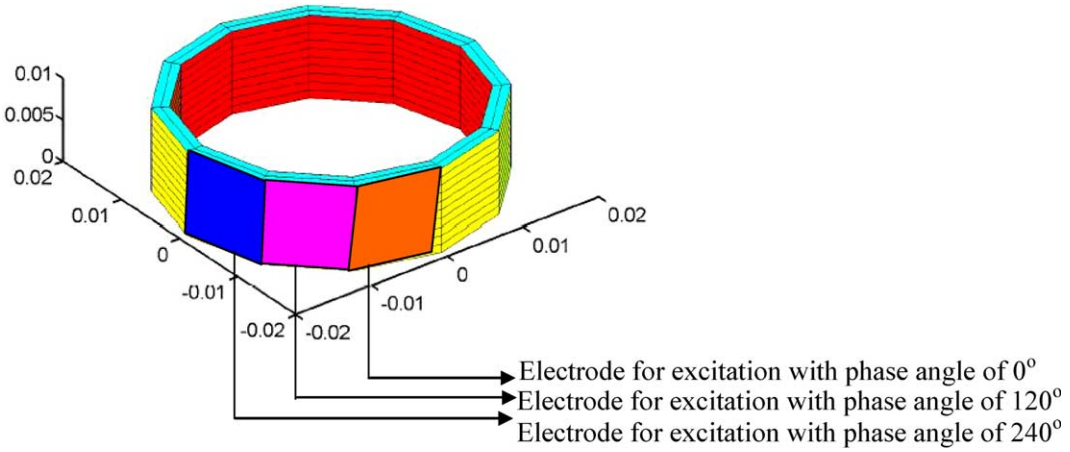

Fig. 5. Finite element mesh used for the piezo-shell alongwith the electrodes for excitation at different phase angles.

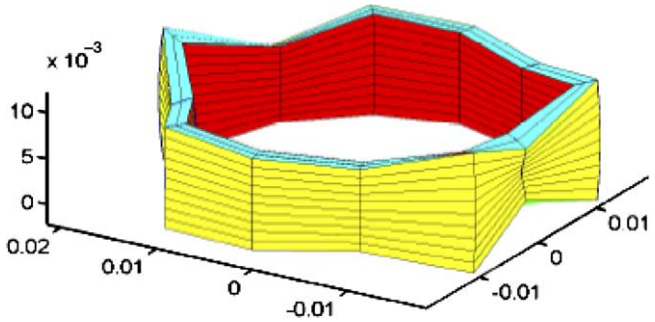

Fig. 6. Mode shape of the piezo-shell used for generating a traveling wave (fundamental longitudinal mode).

Table 3
Comparison of FE calculated frequency for the first two longitudinal modes of piezo-shell with experimental results and Berg et al. (2004)

Mode number	Experimental frequency (kHz)	FEM frequency (kHz)	Shell theory (Berg et al., 2004) frequency (kHz)
1	88.6	89.0	89.0
2	164.2	163.9	159.0

For the purpose of response calculation, proportional damping as well as nonlinear damping methods were used in the analysis and the damping value was taken to be 0.00092 for the first method (obtained from experimental result of velocity versus frequency and by the use of half power method). The results for both proportional and nonlinear damping formulations are same for this material as it has very low damping and this aspect is discussed in detail in Section 4.5. Fig. 7 shows the steady state displacement amplitude calculated using FE simulation and its comparison with experimental results. It can be observed that the FE results match satisfactorily with that of experiment.

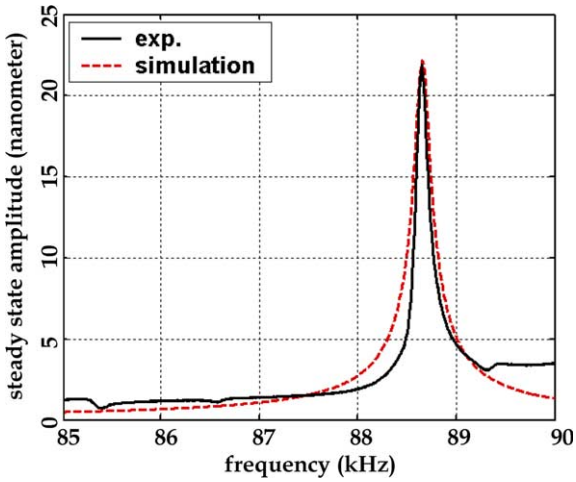

Fig. 7. Comparison of FE simulated steady state displacement amplitude of the piezo-shell with that of experiment.

4.2. Case study 2: Free-free rectangular plate (PIC 181)

The finite element analysis of nonlinear response behaviour of a piezoceramic plate of PIC 181 is presented here. The plate analyzed in this case is a rectangular plate of 70 mm length (L), 20 mm width (W) and 4 mm thickness and is made up of PIC 181 (Figs. 2(b) and 8).

The plate is polarized along the thickness direction. Sinusoidal electric voltages of different amplitudes are applied across the thickness (d_{31} actuation). The first mode of the free-free in-plane vibration of the plate is along its length direction. As this mode is symmetric, symmetric mechanical boundary conditions about length and width direction are applied (i.e., one-fourth of the plate has been analyzed as shown in Fig. 8). As the thickness of the plate is small compared to its length and width, 2D plane stress FE analysis has been used. The electric field is taken as constant throughout the 2D domain. A 5×5 FE mesh has been used (Fig. 8) which consists of 25 4-noded isoparametric 2D quadrilateral elements. This mesh has been used after a convergence study of frequency and displacement response results as described in Section 3.2.

As the electric potential is prescribed on the electrode, only the equation of actuator [first row of Eq. (1)] need be solved. The linear and nonlinear material property matrices have been taken from reference (Parashar and von Wagner, 2004). These material property matrices are obtained using optimization techniques, the details of which are given, for example, in von Wagner and Hagedorn (2002), von Wagner (2003) and

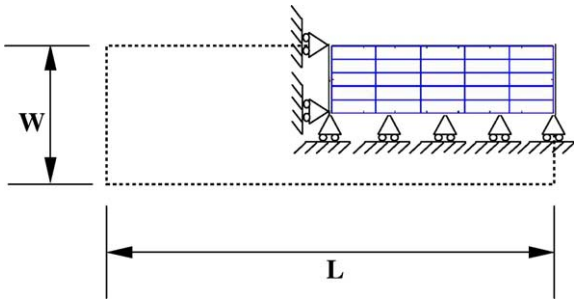

Fig. 8. Symmetric boundary conditions used for first mode of vibration.

Dave (2002). The damping values (proportional damping constants) have been calculated from the experimental results using half-power method. The mass proportional damping constant is assumed zero and the variation of stiffness proportional damping constant with electric field is given in Appendix A2. The material property matrices are given in Appendix A2.

The amplitude of vibration is measured with the help of a laser vibrometer, which is focused along the length onto one end of the plate. A frequency sweep is applied near the first resonance frequency of the plate. The displacement response of the plate for both sweep-up and sweep-down has been compared with experimental results for electrical field excitations of 0.75 and 7.5 V/mm amplitude and these are reported in Figs. 9 and 10, respectively. It was observed that the frequency response path is not same for sweep-up

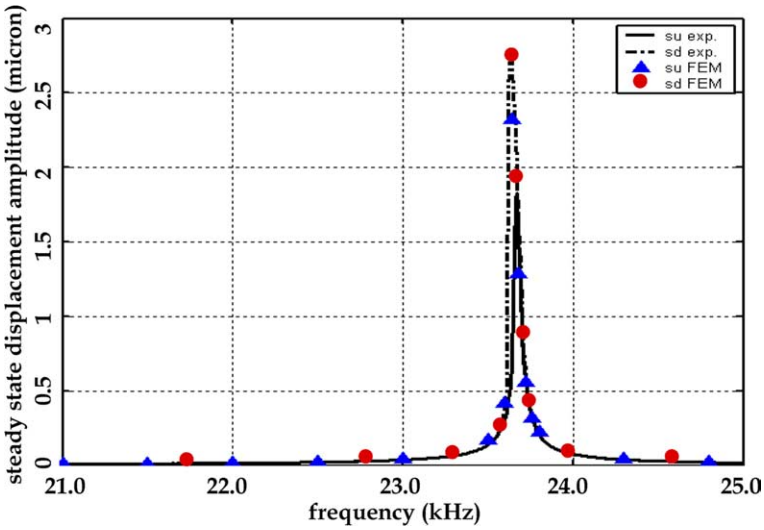

Fig. 9. Comparison of FE predicted and experimental displacement response for PIC 181 plate for a sinusoidal electrical field of 0.75 V/mm peak amplitude.

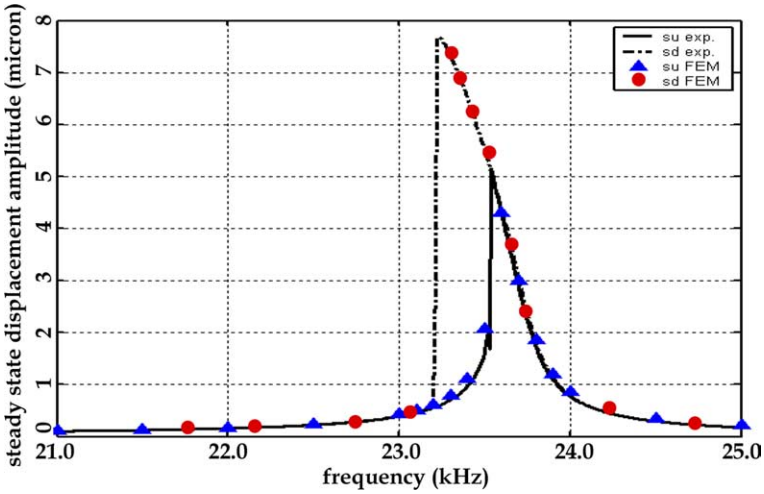

Fig. 10. Comparison of FE predicted and experimental displacement response for PIC 181 plate for a sinusoidal electrical field of 7.5 V/mm peak amplitude.

(frequency is increased) and sweep-down (frequency is decreased) methods of excitation (Fig. 10). The nonlinear softening behaviour and jump phenomena are clearly observed. It may be noted that the results of both proportional damping and nonlinear damping are identical for this low damped material and hence only results of nonlinear damping formulation have been shown in Figs. 9 and 10.

When the system is excited at extremely low electrical field amplitude of 0.75 V/mm, the behaviour is almost linear and there is not much shift in the resonance frequency (Fig. 9) (softening behaviour is not observed). However at slightly higher electric fields, the jump phenomena and bending of response curve towards lower frequencies, etc. (i.e., nonlinear softening) are clearly visible. It can also be observed that the peaks of sweep-up and sweep-down frequency responses are clearly different (Fig. 10). The nonlinear model developed in this work is able to predict all these nonlinear responses satisfactorily for this low damped material. However, for materials, which have high damping property like PIC 255, the jump phenomenon is not observed though the nonlinear softening is prominent. This is discussed in the next section.

4.3. Case study 3: Free-free rectangular plate (PIC 255)

The plate analyzed in this case is a rectangular plate similar to that in case study 2, but of a different material (PIC 255 with higher damping property) and slightly different dimensions, i.e., 70 mm length, 25 mm width and 4 mm thickness. Here also, plane stress analysis was carried out because the thickness is small compared to other dimensions. The boundary conditions (electrical/mechanical) and finite element mesh used are same as those for case study 2. The damping values (proportional damping constants) have been calculated from the experimental results using half-power method. The mass proportional damping constant is assumed zero and the variation of stiffness proportional damping constant with electric field is given in Appendix A3. The material property matrices are given in Appendix A3.

Fast Fourier Transform (FFT) analysis is performed on the measured time domain response data of piezo-plate when a sinusoidal electrical excitation of 7.5 V/mm is applied across the thickness. This is done in order to investigate the presence of signals of frequencies other than the excitation frequency in the response. Fig. 11 shows the FFT analysis of the time domain signal of the laser vibrometer from the piezo-plate when the piezo-plate is excited at one-third of the first natural frequency (this is done in order to excite the first natural frequency due to the inherent nonlinearity present in the system). It can be seen from Fig. 11 that there are two distinct peaks observed in the frequency domain, viz., one at the excitation frequency and the other at a frequency, which is three times the excitation frequency. This gives the evidence that cubic type nonlinearity is dominant in the response of the piezo-plate. Similar observations were also made for PIC 181 plate and PIC 181 cylindrical rods (Samal, 2003).

In order to check the presence of superharmonics in the response spectra as obtained using FE solution procedure, FFT analysis was also carried out on time domain response signal (of FE analysis). Fig. 12 clearly shows a peak at the excitation frequency and another peak at three times the excitation frequency just as observed in the experiment. Hence, cubic type nonlinearity is dominant in the time response and hence the FE model developed in this work has been able to capture this phenomenon satisfactorily.

The displacement response of the plate for both sweep-up and sweep-down has been compared with experimental results for electrical field excitations of 7.5 and 0.75 V/mm amplitudes and these are reported in Figs. 13 and 14, respectively. It is observed from Fig. 13 that the sweep-up and sweep-down responses are nearly identical for this high damped material (unlike the low damped material PIC 181 where they are significantly different). Though the jump phenomenon is not observed, the typical nonlinear softening behaviour (i.e. bending of backbone of frequency response curve towards lower frequency values) is clearly visible. It may be noted that results of nonlinear damping formulation have been shown in Figs. 13 and 14 (as the material is of high damping type). However, the differences between results of proportional and nonlinear damping formulations are discussed in detail in Section 4.5. It can be observed that the nonlinear model developed in this work is able to predict the nonlinear response satisfactorily for this type of

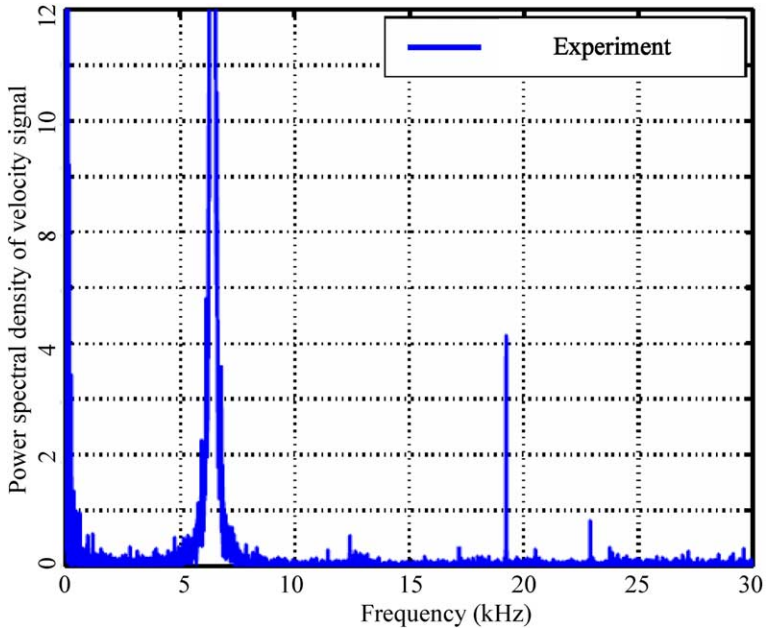

Fig. 11. Experimental FFT of the time domain signal when the plate (PIC 255) is excited at 1/3rd of the first longitudinal natural frequency.

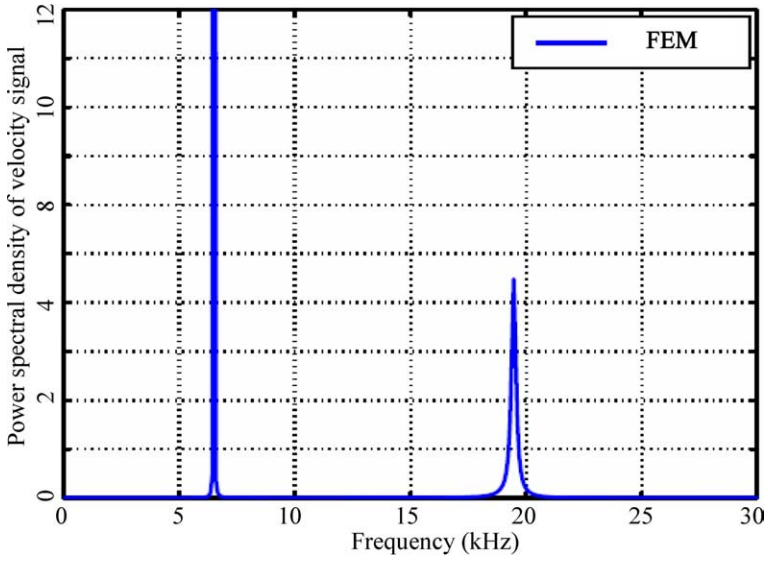

Fig. 12. FFT of the time domain signal when the plate (PIC 255) is excited at 1/3rd of the first longitudinal natural frequency (FEM solution).

material which shows high damping. Similar to the PIC 181 plate, the behaviour of the plate is almost linear and there is no shifting of resonance frequency when the system is excited at extremely low electrical field amplitude of 0.75 V/mm.

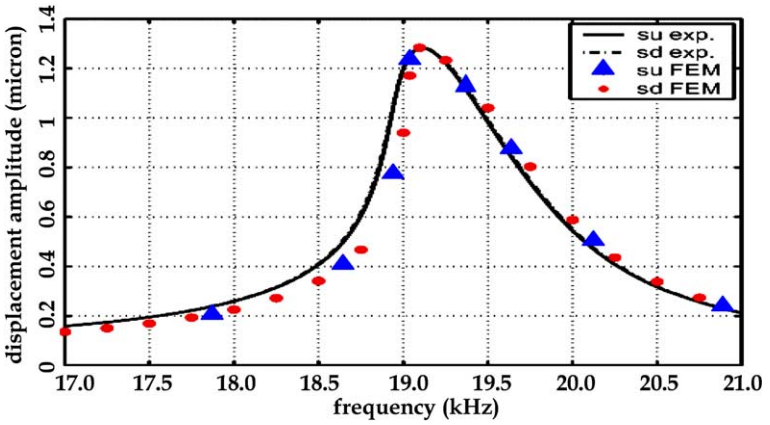

Fig. 13. Comparison of FE predicted and experimental displacement response for PIC 255 plate for electrical field of 7.5 V/mm amplitude.

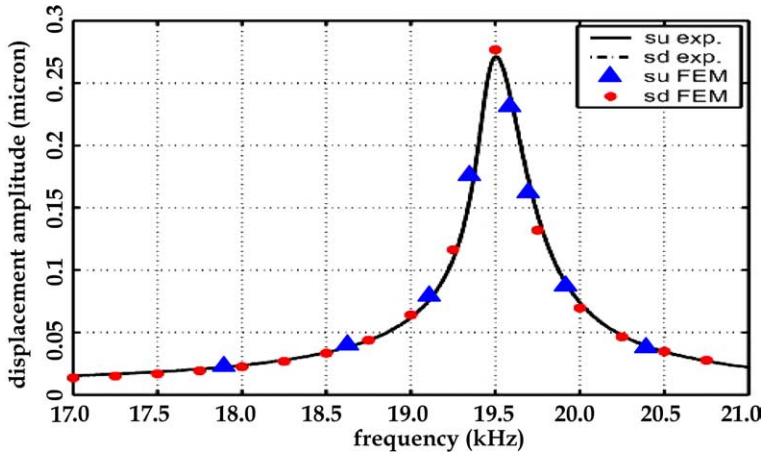

Fig. 14. Comparison of FE predicted and experimental displacement response for PIC 255 plate for electrical field of 0.75 V/mm amplitude.

4.4. Case study 4: Cylindrical piezo-rod (PIC 181)

Analysis has been carried for the cylindrical piezo-rod of 10 mm diameter (D) and 20 mm length (L) made of PIC 181 material. The axisymmetric boundary conditions and the FE mesh used in the analysis are shown in Fig. 15 as the longitudinal vibration of the rod is symmetric about the axis of the cylinder. The rod is vibrating in free-free mode. Hence no mechanical boundary condition was applied in the length direction. A 12×3 FE mesh has been used in the analysis after convergence requirements are satisfied. Plane 2D axisymmetric 4-noded isoparametric elements have been used in the FE analysis. The material properties are given in Appendix A2 for both proportional damping and nonlinear damping formulations. The steady state displacement response of the cylinder is shown in Figs. 16 and 17 for the electrical fields of 1.5 and 0.25 V/mm amplitude, respectively. It may be noted that the results of both proportional damping and nonlinear damping are identical for this low damped material.

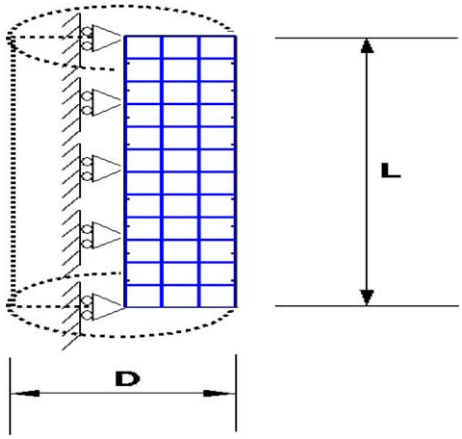

Fig. 15. FE mesh (2D axisymmetric) of the piezocylinder alongwith the boundary condition.

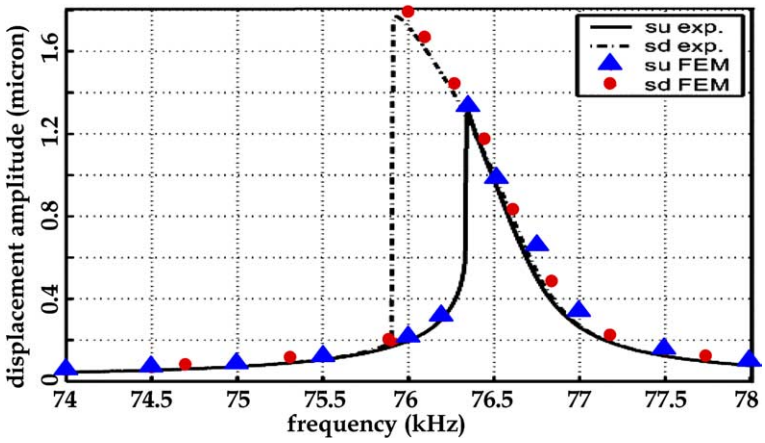

Fig. 16. Comparison of FE predicted and experimental displacement response for PIC 181 rod of 10 mm diameter for electrical field of 1.5 V/mm amplitude.

The results of the FE analysis match very well with experimental results for an electrical excitation of 1.5 V/mm. It is observed that at this electric field, the nonlinearities like jump phenomena and nonlinear softening are prominent. At an extremely low electrical field of 0.25 V/mm amplitude, the response is almost linear and the nonlinear effects are not observed. The maximum displacement amplitude obtained from FE analysis for the electrical excitation of 0.25 V/mm does not agree well with the experimental peak amplitude. The reason for this shortcoming lies in the estimation of damping value for this electric field. The damping values in proportional damping formulation are usually estimated from the experimental responses at certain electric field excitations using half power method and then a best fit relationship is obtained between electric field and the damping constant. In this case, though the best fit damping relationship was able to model the experimental response accurately for the electrical excitation of 1.5 V/mm, it was not able to do so for the case of electrical excitation of 0.25 V/mm. Same deficiency was also observed in the nonlinear damping model where the parameters obtained after optimization were able to model the peak response of 1.5 V/mm excitation accurately, but the agreement between experimental peak and FE peak is

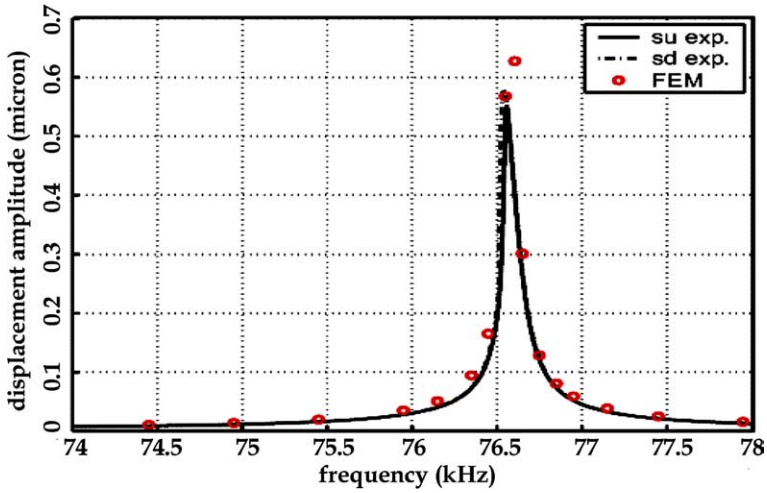

Fig. 17. Comparison of FE predicted and experimental displacement response for PIC 181 rod of 10 mm diameter for electrical field of 0.25 V/mm amplitude.

not very satisfactory. Further investigation into the nonlinear damping model may provide some better insight.

4.5. Comparison of results of proportional damping and nonlinear damping

Analysis of the specimens of different materials has been carried out using both proportional and nonlinear damping formulations. The comparison of results of both analyses for materials PIC 181 and PIC 255 are shown in Figs. 18 and 19, respectively. It can be observed that both models are able to predict

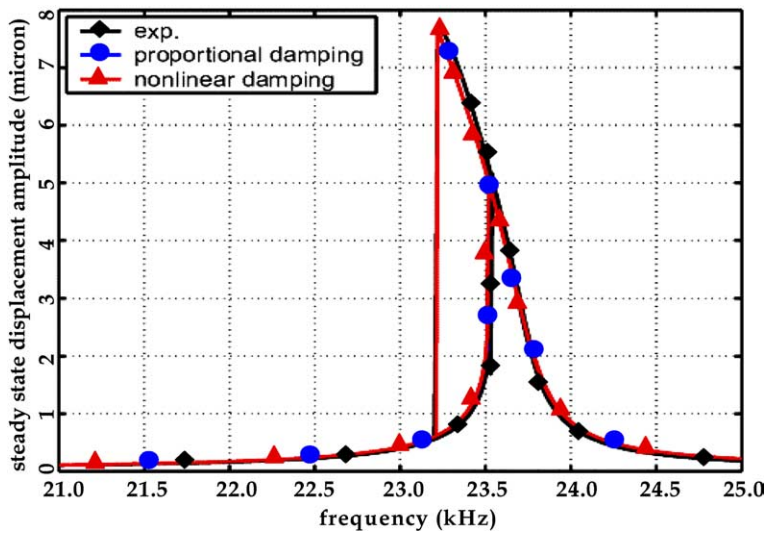

Fig. 18. Comparison of nonlinear response of PIC 181 plate for proportional and nonlinear damping.

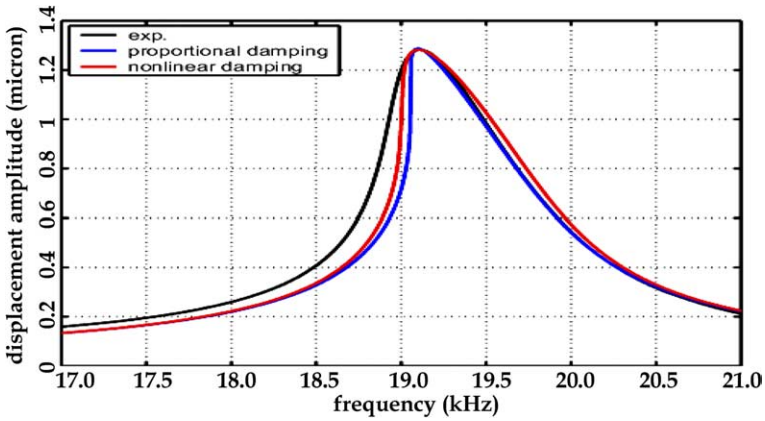

Fig. 19. Comparison of nonlinear response of PIC 255 plate for proportional and nonlinear damping.

the nonlinear displacement response satisfactorily. For the case of low damped materials, both formulations give almost identical results. However, in case of highly damped material like PIC 255 (Fig. 19), the results of nonlinear damping formulation are in better agreement with those of experiment.

The advantage of proportional damping is that it is simple and easy to implement and for material property determination, the number of nonlinear terms to be determined using optimization procedure is less. However, conducting experiments at varying electric fields E is necessary in order to obtain the damping constant as a function of E (refer Figs. 20 and 21) which may require a lot of experimental effort. The advantage of nonlinear damping formulation is that once the material property parameters are determined by optimization procedure, they are fixed and can be used for varying electric field strengths. In this way,

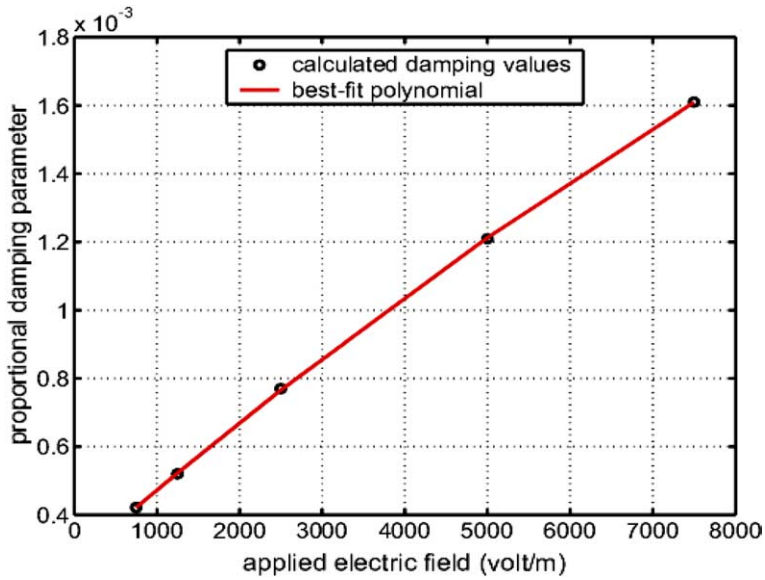

Fig. 20. Variation of stiffness proportional damping constant with the applied electric field for the PIC 181 piezo-plate.

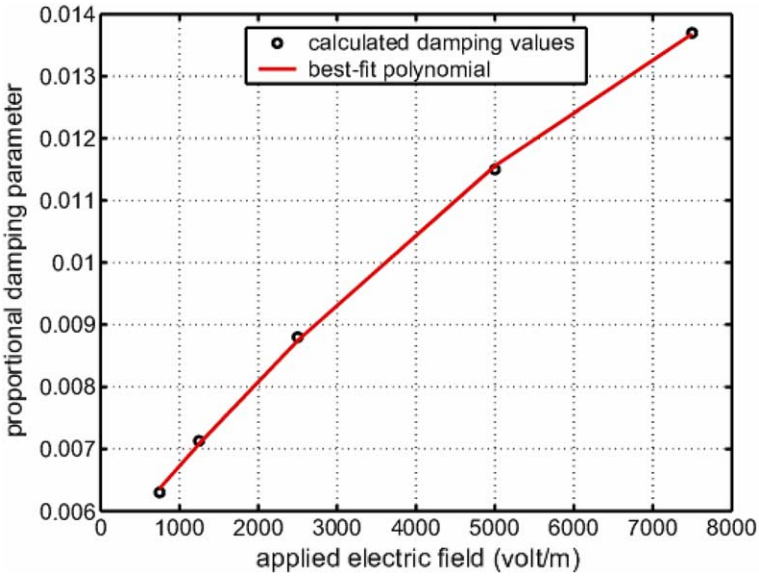

Fig. 21. Variation of stiffness proportional damping constant with applied electric field for the PIC 255 piezo-plate.

these parameters are truly material properties, but it makes the formulation as well as the parameter evaluation by optimization procedure relatively complex.

It may be observed from Figs. 18 and 19 that the frequency response is non-symmetric (about the frequency corresponding to the maximum amplitude) which is a manifestation of the typical nonlinearity in the response. In case of low damped material (Fig. 18), the width of the peak of nonlinear frequency response curve cannot be observed because of presence of jump phenomena whereas in the case of high damped material (Fig. 19), it is clearly visible. It may be observed that the calculated width of peak using nonlinear damping theory is more (Fig. 19) compared to the proportional damping theory and hence the nonlinear damping solution is closer to experimental result as evident from Fig. 19. However, there is still lot of scope for improvement in the nonlinear damping model in order to have a better agreement with the experimental result and the terms considered upto third order in the model may not be adequate. By including higher order terms in the model, the results may further improve which is the scope of further investigation.

5. Conclusion

In a companion paper, the authors proposed generalized expressions for the nonlinear electric enthalpy density function H_{nonl} and the nonlinear virtual work (due to damping forces) $\delta W_{D_{\text{nonl}}}$ (with incorporation of quadratic and cubic terms) and developed the FE model. Experiments have been conducted to study the nonlinear behaviour of piezoelectric materials under weak electric fields on different geometries and different materials. The simulated results for the nonlinear response of four case studies of three different geometries (2D and 3D) and of three different materials (high and low damping type) matched very well with those of experiments for both proportional damping and nonlinear damping formulations. The nonlinear softening behaviour is prominent in the responses of both low and highly damped materials as can be seen from the bending of the backbone curve of nonlinear response. The phenomenon of jump (which is because of presence of cubic nonlinearity) is only evident in low damped materials which is a typical characteristic

of nonlinearity under weak electric fields. For high damped material, the jump phenomenon gets suppressed. However, the nonlinear frequency response especially for the high damped material needs special attention. The presence of higher harmonics was verified by conducting FFT analysis on both the experimental and FE time domain responses and this clearly shows the dominance of cubic nonlinearity in the response. Hence, the nonlinear finite element formulation, based on generalization of electric enthalpy and virtual work (by damping forces) to quadratic and cubic order terms is very helpful in predicting the nonlinear frequency responses under weak electric when excited near a structural mode. It can be used for designing and optimizing the performance of various piezoelectric material systems operating near resonance such as those found in ultrasonic applications.

The nonlinear damping improves the FE results for the material with high damping whereas for the material with low damping, both proportional and nonlinear damping formulations give almost same results. It may be noted the frequency response is non-symmetric about the maximum amplitude and the width of the peak is more in experiment compared to the FE simulation. The results of nonlinear damping are better compared to that proportional damping in the sense that it is able to pick the tendency of peak broadening as observed in the experiment. However, the third order nonlinear terms considered in the nonlinear damping formulation in the present investigation may not be sufficient to capture the experimental behaviour very accurately and hence one needs to further refine the nonlinear damping terms by including higher order terms which is the scope of further investigation.

Acknowledgements

The authors are grateful to the German Academic Exchange Service (DAAD) for providing a fellowship to Mr. M.K. Samal to carry out part of his thesis work at Darmstadt University of Technology, Germany. This work is supported by the Deutsche Forschungs Gemeinschaft vide research grant Ha1060/36. The first two authors gratefully acknowledge the support received from Aeronautics Research and Development Board and Department of Science and Technology, India.

Appendix A1. Material properties of PIC 141

The material property matrices for PIC141, PIC 181 and PIC255 were obtained by optimization of the closed form solution of a simple geometry with experimental results (Parashar and von Wagner, 2004). The significant properties are given in these appendices. It was observed that the other nonlinear material properties had negligible effect. In the case of nonlinear damping formulation, certain additional material damping property matrices are required and these are also provided here.

$$[S^E] = \begin{bmatrix} 1.4220 & -0.4530 & -0.4530 & 0 & 0 & 0 \\ -0.4530 & 1.4490 & -0.4720 & 0 & 0 & 0 \\ -0.4530 & -0.4720 & 1.4490 & 0 & 0 & 0 \\ 0 & 0 & 0 & 3.275 & 0 & 0 \\ 0 & 0 & 0 & 0 & 3.275 & 0 \\ 0 & 0 & 0 & 0 & 0 & 3.275 \end{bmatrix} \times 10^{-11}\ \mathrm{m^2/N}$$

$$[d] = \begin{bmatrix} 0 & 0 & 0 & 0 & 4.75 & 0 \\ 0 & 0 & 0 & 4.75 & 0 & 0 \\ -1.15 & -1.15 & 3.30 & 0 & 0 & 0 \end{bmatrix} \times 10^{-10}\ \mathrm{m/V}$$

$$[C_{21}] = -\begin{bmatrix} 9.2000 & 4.8700 & 4.8700 & 0 & 0 & 0 \\ 4.8700 & 9.2000 & 4.3500 & 0 & 0 & 0 \\ 4.8700 & 4.3500 & 8.7520 & 0 & 0 & 0 \\ 0 & 0 & 0 & 1.1020 & 0 & 0 \\ 0 & 0 & 0 & 0 & 1.1020 & 0 \\ 0 & 0 & 0 & 0 & 0 & 1.3140 \end{bmatrix} \times 10^{16}\ \mathrm{N/m^2}$$

Additional matrices for nonlinear damping formulation

$$[C_d^{(0)}] = -\begin{bmatrix} 635 & 545 & 497 & 0 & 0 & 0 \\ 545 & 635 & 497 & 0 & 0 & 0 \\ 497 & 497 & 590 & 0 & 0 & 0 \\ 0 & 0 & 0 & 172 & 0 & 0 \\ 0 & 0 & 0 & 0 & 172 & 0 \\ 0 & 0 & 0 & 0 & 0 & 185 \end{bmatrix} \mathrm{N\ s/m}$$

$$[C_{d1}^{(2)}] = -\begin{bmatrix} 3.9200 & 2.9805 & 2.7500 & 0 & 0 & 0 \\ 2.9805 & 3.9200 & 2.7500 & 0 & 0 & 0 \\ 2.7500 & 2.7500 & 3.5400 & 0 & 0 & 0 \\ 0 & 0 & 0 & 0.765 & 0 & 0 \\ 0 & 0 & 0 & 0 & 0.765 & 0 \\ 0 & 0 & 0 & 0 & 0 & 0.928 \end{bmatrix} \times 10^{10}\ \mathrm{N\ s/m^2}$$

Appendix A2. Material properties of PIC 181

$$[S^E] = \begin{bmatrix} 1.1600 & -0.4070 & -0.4996 & 0 & 0 & 0 \\ -0.4070 & 1.1750 & -0.4996 & 0 & 0 & 0 \\ -0.4996 & -0.4996 & 1.4110 & 0 & 0 & 0 \\ 0 & 0 & 0 & 3.5330 & 0 & 0 \\ 0 & 0 & 0 & 0 & 3.5330 & 0 \\ 0 & 0 & 0 & 0 & 0 & 3.1640 \end{bmatrix} \times 10^{-11}\ \mathrm{m^2/N}$$

$$[d] = \begin{bmatrix} 0 & 0 & 0 & 0 & 3.89 & 0 \\ 0 & 0 & 0 & 3.89 & 0 & 0 \\ -1.148 & -1.148 & 2.53 & 0 & 0 & 0 \end{bmatrix} \times 10^{-10}\ \mathrm{m/V}$$

$$[C_{21}] = -\begin{bmatrix} 4.7000 & 2.7914 & 2.6525 & 0 & 0 & 0 \\ 2.7914 & 4.7000 & 2.6525 & 0 & 0 & 0 \\ 2.6525 & 2.6525 & 3.9978 & 0 & 0 & 0 \\ 0 & 0 & 0 & 0.8465 & 0 & 0 \\ 0 & 0 & 0 & 0 & 0.8465 & 0 \\ 0 & 0 & 0 & 0 & 0 & 0.9452 \end{bmatrix} \times 10^{16}\ \mathrm{N/m^2}$$

Additional matrices require for nonlinear damping formulation

$$[C_d^{(0)}] = -\begin{bmatrix} 291 & 173 & 164 & 0 & 0 & 0 \\ 173 & 291 & 164 & 0 & 0 & 0 \\ 164 & 164 & 248 & 0 & 0 & 0 \\ 0 & 0 & 0 & 52.5 & 0 & 0 \\ 0 & 0 & 0 & 0 & 52.5 & 0 \\ 0 & 0 & 0 & 0 & 0 & 58.5 \end{bmatrix} \text{N s/m}$$

$$[C_{d1}^{(2)}] = -\begin{bmatrix} 2.1800 & 1.2947 & 1.2303 & 0 & 0 & 0 \\ 1.2947 & 2.1800 & 1.2303 & 0 & 0 & 0 \\ 1.2303 & 1.2303 & 1.8543 & 0 & 0 & 0 \\ 0 & 0 & 0 & 0.3926 & 0 & 0 \\ 0 & 0 & 0 & 0 & 0.3926 & 0 \\ 0 & 0 & 0 & 0 & 0 & 0.4384 \end{bmatrix} \times 10^{10} \text{ N s/m}^2$$

Appendix A3. Material properties of PIC 255 plate

$$[S^E] = \begin{bmatrix} 1.7160 & -0.4842 & -0.7050 & 0 & 0 & 0 \\ -0.4070 & 1.6170 & -0.7050 & 0 & 0 & 0 \\ -0.7050 & -0.7050 & 2.0700 & 0 & 0 & 0 \\ 0 & 0 & 0 & 5.2370 & 0 & 0 \\ 0 & 0 & 0 & 0 & 5.2370 & 0 \\ 0 & 0 & 0 & 0 & 0 & 4.2020 \end{bmatrix} \times 10^{-11} \text{ m}^2/\text{N}$$

$$[d] = \begin{bmatrix} 0 & 0 & 0 & 0 & 5.00 & 0 \\ 0 & 0 & 0 & 5.00 & 0 & 0 \\ -1.65 & -1.65 & 4.00 & 0 & 0 & 0 \end{bmatrix} \times 10^{-10} \text{ m/V}$$

$$[C_{21}] = -\begin{bmatrix} 1.3000 & 0.6380 & 0.6600 & 0 & 0 & 0 \\ 0.6380 & 1.3000 & 0.6600 & 0 & 0 & 0 \\ 0.6600 & 0.6600 & 1.1532 & 0 & 0 & 0 \\ 0 & 0 & 0 & 0.2781 & 0 & 0 \\ 0 & 0 & 0 & 0 & 0.2781 & 0 \\ 0 & 0 & 0 & 0 & 0 & 0.3466 \end{bmatrix} \times 10^{18} \text{ N/m}^2$$

Additional matrices required for nonlinear damping formulation

$$[C_d^{(0)}] = -\begin{bmatrix} 5670 & 2783 & 2879 & 0 & 0 & 0 \\ 2783 & 5670 & 2879 & 0 & 0 & 0 \\ 2879 & 2879 & 5030 & 0 & 0 & 0 \\ 0 & 0 & 0 & 1213 & 0 & 0 \\ 0 & 0 & 0 & 0 & 1213 & 0 \\ 0 & 0 & 0 & 0 & 0 & 1512 \end{bmatrix} \text{N s/m}$$

$$[C_{d1}^{(2)}] = -\begin{bmatrix} 4.1000 & 2.0121 & 2.0817 & 0 & 0 & 0 \\ 2.0121 & 4.1000 & 2.0817 & 0 & 0 & 0 \\ 2.0817 & 2.0204 & 3.6372 & 0 & 0 & 0 \\ 0 & 0 & 0 & 0.8772 & 0 & 0 \\ 0 & 0 & 0 & 0 & 0.8772 & 0 \\ 0 & 0 & 0 & 0 & 0 & 1.0932 \end{bmatrix} \times 10^{12} \text{ N s/m}^2$$

$$\gamma_{21} = \begin{bmatrix} 0 & 0 & 0 & 0 & -1.2745 & 0 \\ 0 & 0 & 0 & -1.2745 & 0 & 0 \\ 0.5987 & 0.6897 & -2.1407 & 0 & 0 & 0 \end{bmatrix} \times 10^{8} \text{ N/m/V}$$

$$\gamma_{0d} = \begin{bmatrix} 0 & 0 & 0.2169 \\ 0 & 0 & 0.2499 \\ 0 & 0 & -0.7756 \\ 0 & -0.4617 & 0 \\ -0.4617 & 0 & 0 \\ 0 & 0 & 0 \end{bmatrix} \times 10^{-6} \text{ N s/m/V}$$

$$\gamma_{2d}^{(1)} = \begin{bmatrix} 0 & 0 & 0.1784 \\ 0 & 0 & 0.2055 \\ 0 & 0 & -0.6379 \\ 0 & -0.3798 & 0 \\ -0.3798 & 0 & 0 \\ 0 & 0 & 0 \end{bmatrix} \text{N s/m/V}$$

References

Beige, H., Schmidt, G., 1982. Electromechanical resonances for investigating linear and nonlinear properties of dielectrics. Ferroelectrics 41, 39–49.

Berg, M., Hagedorn, P., Gutschmidt, S., 2004. On the dynamics of piezoelectric cylindrical shells. Journal of Sound and Vibration 274 (1–2), 91–109.

Dave, H., 2002. Longitudinal vibrations of piezoceramics subjected to weak electric fields: experiment and modelling, Masters Thesis, Institut fuer mechanik, Technische Universitaet Darmstadt, Germany.

Flügge, W., 1962. Statik und Dynamic der Schalen. Springer-Verlag, Berlin.

Flügge, W., 1973. Stresses in Shells, second ed. Springer-Verlag, Berlin.

Parashar, S.K., von Wagner, U., 2004. Nonlinear Dynamics 37, 51–73.

Samal, M.K., 2003. Modelling of nonlinear behaviour of piezoelectric materials under weak electric fields. Masters Thesis, Department of Mechanical Engineering, Indian Institute of Technology, Bombay.

Samal, M.K., Seshu, P., Parashar, S.K., von Wagner, U., Hagedorn, P., Dutta, B.K., Kushwaha, H.S., 2005. Nonlinear behaviour of piezoceramics under weak electric fields, Part-I: 3-D finite element formulation (to appear in International Journal of Solids and Structures).

Sun, D., Tong, L., Wang, D., 2004. An incremental algorithm for static shape control of smart structures with nonlinear piezoelectric actuators. International Journal of Solids and Structures 41, 2277–2292.

von Wagner, U., Hagedorn, P., 2002. Piezo-beam-systems subjected to weak electric field: experiment and modelling of nonlinearities. Journal of Sound and Vibration 256 (5), 861–872.

von Wagner, U., 2003. Non-linear longitudinal vibrations of piezoceramics excited by weak electric fields. International Journal of Non-linear Mechanics 38, 565–574.

von Wagner, U., 2004. Non-linear longitudinal vibrations of non-slender piezoceramic rods. International Journal of Non-linear Mechanics 39, 673–688.

Zhou, Y.H., Tzou, H.S., 2000. Active control of nonlinear piezoelectric circular shallow spherical shells. International Journal of Solids and Structures 37 (12), 1663–1677.